Over-improved stout-link smearing

Peter J. Moran and Derek B. Leinweber

Special Research Centre for the Subatomic Structure of Matter (CSSM), Department of Physics, University of Adelaide 5005, Australia

(Received 8 January 2008; revised manuscript received 19 February 2008; published 5 May 2008)

A new over-improved stout-link smearing algorithm, designed to stabilize instanton-like objects, is presented. A method for quantifying the selection of the over-improvement parameter, ϵ, is demonstrated. The new smearing algorithm is compared with the original stout-link smearing, and Symanzik improved smearing through calculations of the topological charge and visualizations of the topological charge density. We find the incorporation of improvement in stout-link smearing to be essential for the accurate study of QCD vacuum structure.

DOI: 10.1103/PhysRevD.77.094501 PACS numbers: 12.38.Gc, 11.15.Ha, 12.38.Aw

I. INTRODUCTION

Studies of long distance physics in lattice QCD simulations often require the suppression of short-range UV fluctuations. This is normally achieved through the application of a smoothing algorithm. The most common prescriptions are cooling [1–3], APE [4,5], and improved APE smearing [6], HYP smearing [7], and more recently, EXP or stout-link smearing [8] and LOG smearing [9]. Filtering methods such as these are also used regularly in calculations of physical observables to improve overlap with low energy states.

All smoothing methods are based on an approximation to the continuum gluonic action

$$S_g = \frac{1}{2}\int d^4x \,\mathrm{tr}[F_{\mu\nu}F_{\mu\nu}]. \tag{1}$$

Because space-time is approximated by a 4D lattice, these approximations contain unavoidable discretization errors. These errors can have a negative effect on the topological objects present in the gauge field being studied and are detrimental to the smoothing process.

There are two noteworthy approaches for dealing with these discretization errors and both have been restricted to cooling algorithms. One approach is to eliminate the discretization errors through a strategic combination of larger Wilson loops [6,10–12] leading to the so-called 3-, 4-, and 5-loop $\mathcal{O}(a^4)$-improved actions. These actions are used in the cooling algorithm to identify the individual link that will maximally reduce the local action. The difficulty with this approach is that relatively long link paths are combined with the plaquette in improving the action. The preferred 3- and 5-loop improved actions include the 3×3 Wilson loop which involves 8 links more than the plaquette. Early in the application of cooling, it is essential to accommodate for the large renormalizations of the improvement coefficients and the best practice [12] is to consider tadpole improvement via the mean link, u_0. However, early in the cooling procedure, a mean-field estimate of $1/u_0^8$ for the coefficient renormalization is not accurate and the utility of highly improved actions on rough configurations is of concern.

Ideally one seeks a solution involving only the most local link paths, the plaquette and the rectangle. Unfortunately, as shown by Perez, *et al.* [13] and briefly reiterated below, the $\mathcal{O}(a^4)$ errors remaining after the removal of the $\mathcal{O}(a^2)$ errors act to spoil instanton-like objects in the field. They proposed the second noteworthy approach of over-improved cooling as a means of taming these errors via the introduction of a new tunable parameter ϵ into their action [13]. They selected the combination of 1×1 and 2×2 link paths, exacerbating problems associated with the renormalization of the coefficients.

Thus, there is a need to investigate the utility of over-improvement in the maximally local case of 1×1 and 1×2 link paths. Here the standard tactics of tadpole improvement will be most effective. To the best of our knowledge this is the first derivation of the over-improved 1×1 plus 1×2 action and as such, the first investigation of its utility in both classical instanton configurations and in preserving topological structure in lattice Monte Carlo generated configurations.

We also note that there has been remarkably little, if any, focus on the role of improvement and over-improvement in the context of smearing algorithms. As such this paper leads an important new area of study and presents the first application of (over-)improvement in the popular stout-link smearing algorithm.

Smearing is preferred to cooling for several reasons. Unlike cooling, smearing provides a well-defined and differentiable lattice action suitable for use in dynamical-fermion simulations. Moreover, the presence of a smearing parameter enables a more extensive control over the amount of smoothing performed in the important early stages of the smoothing process.

In Sec. II we begin by presenting a brief summary of the most common smoothing algorithms and illustrate the role of the lattice action in both cooling and smearing. We then describe the creation of a new over-improved stout-link smearing algorithm based on 1×1 plus 1×2 paths in

Sec. III. Here, the lattice discretization errors of a single classical instanton are considered. As emphasized above, this is the first exploration of over-improvement utilizing the maximally local 1×1 and 1×2 link paths.

In Sec. IV we present the first quantitative method for tuning the over-improvement parameter, ϵ. This is essential to ensuring topological objects larger than the dislocation threshold are not distorted under continued smearing. Whereas the previous study [13] simply selected the value of -1, we have discovered this choice is less than optimal.

Finally, in Sec. V we demonstrate the utility of the over-improved stout-link smearing algorithm on a variety of lattices, including large $28^3 \times 96$ light dynamical gauge fields from the MILC collaboration [14,15]. Of particular note is our illustration of the destruction of topologically nontrivial objects in real gauge field configurations under standard stout-link smearing and the preservation of these objects under over-improved stout-link smearing. To the best of our knowledge, this is the first time such a comparison has been illustrated using any (over-)improved smoothing algorithm.

II. SMOOTHING ALGORITHMS

Standard cooling proceeds via a systematic sequential update of all links $U_\mu(x)$ on the lattice, where at each link update the local Wilson action [16] is minimized. The local Wilson action corresponding to $U_\mu(x)$ is defined as

$$S_W(x) = \beta \sum_{\substack{\nu \\ \nu \neq \mu}} \frac{1}{3} \operatorname{Re} \operatorname{tr}[1 - U_\mu(x)\Sigma_{\mu\nu}(x)], \tag{2}$$

where

$$\Sigma_{\mu\nu}(x) = U_\nu(x+\hat{\mu})U_\mu^\dagger(x+\hat{\nu})U_\nu^\dagger(x) + U_\nu^\dagger(x+\hat{\mu}-\hat{\nu})U_\mu^\dagger(x-\hat{\nu})U_\nu(x-\hat{\nu}) \tag{3}$$

is the sum of the two staples touching $U_\mu(x)$ which reside in the μ-ν plane. From Eq. (2), we can see that S_W will be minimized when $\operatorname{Re} \operatorname{tr}[1 - U_\mu(x)\Sigma_{\mu\nu}(x)] = 0$. It naturally follows that, when cooling, the aim is to replace $U_\mu(x)$ with a new link that optimizes

$$\max \operatorname{Re} \operatorname{tr}\left(U_\mu(x) \sum_{\substack{\nu \\ \nu \neq \mu}} \Sigma_{\mu\nu}(x) \right). \tag{4}$$

When performing this update in parallel, one must be careful not to replace any link which is included in the local action of a neighboring link. This requirement means that cooling is a relatively slow operation computationally, but fast in regard to the removal of action from the gauge field.

APE smearing differs from standard cooling in that all links can be simultaneously updated in a single sweep through the lattice, resulting in a significant speed increase. In APE smearing, one first calculates a smeared link $U'_\mu(x)$, which is the weighted sum of its nearest neighbors,

$$U'_\mu(x) = (1-\alpha)U_\mu(x) + \frac{\alpha}{6} \sum_{\substack{\nu \\ \nu \neq \mu}} \Sigma^\dagger_{\mu\nu}(x), \tag{5}$$

where $\Sigma_{\mu\nu}$ is defined as in Eq. (3), and α is a real parameter, usually set to ≈ 0.7. The new link $U'_\mu(x)$ is then projected back into the SU(3) group via some projection operator $\mathcal{P}$,

$$\tilde{U}_\mu(x) = \mathcal{P} U'_\mu(x). \tag{6}$$

The projection of Eq. (6) is necessary because we have performed an additive step in Eq. (5), which is not an SU(3) group operation. The projection step is not uniquely defined, but the preferred method is to select the new smeared link $U_\mu(x)$ such that it maximizes

$$\operatorname{Re} \operatorname{tr}(U_\mu(x) U'^\dagger_\mu(x)). \tag{7}$$

In the limit $\alpha \to 1$ we see that Eq. (5) becomes

$$U'_\mu(x) \to \frac{1}{6} \sum_{\substack{\nu \\ \nu \neq \mu}} \Sigma^\dagger_{\mu\nu}(x). \tag{8}$$

Substituting this result into Eq. (7) shows how the projection method has become equivalent to cooling equation (4), and that there exists a direct link between APE smearing and cooling in the limit that links are updated sequentially. The simultaneous update of APE smearing limits $\alpha < 0.75$ [17].

The more recent smearing technique, stout-link smearing [8], makes use of the exponential function to remain within the gauge group and remove the need for a projection step. Beginning with the staples equation (3), define

$$C_\mu(x) = \sum_{\substack{\nu \\ \nu \neq \mu}} \rho_{\mu\nu} \Sigma^\dagger_{\mu\nu}(x), \tag{9}$$

where we will choose an isotropic four-dimensional constant $\rho_{\mu\nu} = \rho_{\mathrm{sm}}$, but other selections are possible. The matrix $Q_\mu(x)$ defined by

$$Q_\mu(x) = \frac{i}{2}(\Omega^\dagger_\mu(x) - \Omega_\mu(x)) - \frac{i}{6} \operatorname{tr}(\Omega^\dagger_\mu(x) - \Omega_\mu(x)), \tag{10}$$

with

$$\Omega_\mu(x) = C_\mu(x) U^\dagger_\mu(x), \tag{11}$$

is by definition Hermitian and traceless, and hence $e^{iQ_\mu(x)} \in \mathrm{SU}(3)$. The new smeared link is then defined by

$$\tilde{U}_\mu(x) = \exp(iQ_\mu(x)) U_\mu(x). \tag{12}$$

An expansion of the exponential in Eq. (12) results in the same sum of paths, to first order in ρ_{sm}, as for APE smearing [8]. Given this, and the already established link between APE smearing and cooling, it follows that there exists a connection between cooling and stout-link smear-

ing. Indeed, simulations of lattice QCD show that for any given gauge field, the structures revealed by the smoothing procedures are remarkably similar.

III. DISCRETIZATION ERRORS AND IMPROVEMENT

The corrosion of topological structures during the smoothing process is a well known side effect of both cooling and smearing [6,11,12]. It is the unavoidable discretization errors in the lattice action that are the cause of this observed behavior. This obviously inhibits our ability to study the topological excitations on the lattice with the most local operators and it would be beneficial if it could be prevented.

When a gauge field is smoothed, the topological structures within are subjected to the effects of lattice discretization errors. One such topological excitation is the instanton. To understand how the errors will alter instanton distributions, first consider the clover Wilson action given by

$$S_W = \beta \sum_x \sum_{\mu>\nu} (1 - P_{\mu\nu}(x)), \tag{13}$$

where $P_{\mu\nu}(x)$ denotes $1/3$ of the real trace of the clover average of the four plaquettes touching the point x.

Following Ref. [13], S_W can be expanded in powers of the lattice spacing, a, giving

$$\begin{aligned} S_W = a^4 \sum_x \sum_{\mu>\nu} \mathrm{tr}\Big[& \frac{1}{2} F_{\mu\nu}^2(x) - \frac{a^2}{24}((\mathcal{D}_\mu F_{\mu\nu}(x))^2 \\ & + (\mathcal{D}_\nu F_{\mu\nu}(x))^2) - \frac{a^4}{24}\Big(g^2 F_{\mu\nu}^4(x) \\ & - \frac{1}{30}((\mathcal{D}_\mu^2 F_{\mu\nu}(x))^2 + (\mathcal{D}_\nu^2 F_{\mu\nu}(x))^2) \\ & - \frac{1}{3}\mathcal{D}_\mu^2 F_{\mu\nu}(x)\mathcal{D}_\nu^2 F_{\mu\nu}(x) + \frac{1}{4}(\mathcal{D}_\mu \mathcal{D}_\nu F_{\mu\nu}(x))^2\Big)\Big] \\ & + O(a^{10}, g^4), \end{aligned} \tag{14}$$

where $igF_{\mu\nu} = [D_\mu, D_\nu]$, $D_\mu = \partial_\mu + igA_\mu$, and $\mathcal{D}_\mu \phi = [D_\mu, \phi]$, for arbitrary ϕ.

The goal is to substitute the instanton solution [18] given by

$$A_\mu(x) = \frac{x^2}{x^2 + \rho_{\mathrm{inst}}^2}\left(\frac{i}{g}\right)\partial_\mu(S)S^{-1}, \tag{15}$$

where

$$S \equiv \frac{x_4 \pm i\vec{x}\cdot\vec{\sigma}}{\sqrt{x^2}}, \tag{16}$$

for instantons/anti-instantons with σ the Pauli matrices, into the expanded Wilson action equation (14). This requires the use of the lattice approximation $a^4\sum_x \approx \int d^4x$. Substituting the instanton solution equation (15) into Eq. (14) and performing the integration then yields

$$S_W^{\mathrm{inst}} = \frac{8\pi^2}{g^2}\left[1 - \frac{1}{5}\left(\frac{a}{\rho_{\mathrm{inst}}}\right)^2 - \frac{1}{70}\left(\frac{a}{\rho_{\mathrm{inst}}}\right)^4\right]. \tag{17}$$

Notice that the leading error term in Eq. (17) is negative and depends upon the instanton size ρ_{inst}. When the Wilson action is used in a smoothing algorithm these errors result in an underestimation of the action density. Additionally, by decreasing ρ_{inst} the action will be further reduced. The smoothing algorithms, which are trying to decrease the action, will therefore shrink ρ_{inst} in order to reduce the action. Repeated application of the smoothing procedures will eventually lead to overwhelming discretization errors and cause instantons to "fall through the lattice" and disappear.

Improved actions aim to fix the problem of discretization errors by including different sized Wilson loops in the calculation of the action. By choosing the coefficients of the loop combinations carefully, it is possible to eliminate the leading order error terms.

The Symanzik improved action uses a linear combination of plaquette and rectangular loops to eliminate the $O(a^2)$ errors:

$$\begin{aligned} S_S = \beta \sum_x \sum_{\mu>\nu} \Big[& \frac{5}{3}(1 - P_{\mu\nu}(x)) - \frac{1}{12}((1 - R_{\mu\nu}(x)) \\ & + (1 - R_{\nu\mu}(x)))\Big]. \end{aligned} \tag{18}$$

Analogous to $P_{\mu\nu}$, $R_{\mu\nu}$ and $R_{\nu\mu}$ denote the different possible orientations of the rectangular loops.

This can be expanded in terms of a, and the instanton solution substituted as above to find, in agreement with [13], that

$$S_S^{\mathrm{inst}} = \frac{8\pi^2}{g^2}\left[1 - \frac{17}{210}\left(\frac{a}{\rho_{\mathrm{inst}}}\right)^4\right]. \tag{19}$$

The $O(a^2)$ error term has been removed by design, but we see that the $O(a^4)$ term is still negative. Therefore, this action will still not preserve instantons.

IV. OVER-IMPROVEMENT

A. Formalism

In 1993, Perez *et al.* [13] introduced the notion of over-improved cooling, also known as ϵ-cooling. The essential idea was that, instead of trying to use different loop combinations to completely eliminate higher order error terms, they would instead choose their coefficients such that the leading error terms become positive.

Introducing the parameter ϵ, they defined the following action:

$$S_P(\epsilon) = \beta \sum_x \sum_{\mu>\nu} \left[\frac{4-\epsilon}{3}(1 - P_{\mu\nu}(x)) + \frac{\epsilon - 1}{48}(1 - W_{\mu\nu}(x)) \right], \quad (20)$$

where $W_{\mu\nu}(x)$ denotes the clover average of the 2×2 squares (windows) touching the point x. Note that in Eq. (20), ϵ has been introduced such that $\epsilon = 1$ gives the standard Wilson action and $\epsilon = 0$ results in an $O(a^2)$ improved action. Expanding Eq. (20) in terms of a and substituting the instanton solution equation (15) gives

$$S_P^{\text{inst}} = \frac{8\pi^2}{g^2}\left[1 - \frac{\epsilon}{5}\left(\frac{a}{\rho_{\text{inst}}}\right)^2 + \frac{4 - 5\epsilon}{70}\left(\frac{a}{\rho_{\text{inst}}}\right)^4 \right], \quad (21)$$

where the $O(a^2)$ term is directly proportional to $-\epsilon$. Thus, by making $\epsilon < 0$, the leading order discretization errors become positive, and the modified action should preserve instantons.

In the interests of preserving locality, we choose to use the traditional combination of plaquettes and rectangles as in the Symanzik improved action in preference to the combination of the 1×1 and 2×2 loops used in [13]. As emphasized in the Introduction, this has the benefit of reducing the coefficient renormalization that is applied to the link paths, because of the smaller difference in the number of links utilized. This then enables precision tuning of ϵ.

We now introduce the parameter ϵ into the Symanzik improved action equation (18). By requiring that $\epsilon = 0$ gives the $O(a^2)$ improved Symanzik action, and that $\epsilon = 1$ gives the standard Wilson action. This implies the following form for the action:

$$S(\epsilon) = \beta \sum_x \sum_{\mu>\nu} \left[\frac{5 - 2\epsilon}{3}(1 - P_{\mu\nu}(x)) - \frac{1 - \epsilon}{12}((1 - R_{\mu\nu}(x)) + (1 - R_{\nu\mu}(x))) \right]. \quad (22)$$

Performing the expansion in a gives

$$S(\epsilon) = a^4 \sum_x \sum_{\mu>\nu} \text{tr}\left[\frac{1}{2}F_{\mu\nu}^2(x) - \frac{\epsilon a^2}{24}((\mathcal{D}_\mu F_{\mu\nu}(x))^2 + (\mathcal{D}_\nu F_{\mu\nu}(x))^2) + \frac{a^4}{24}\left(g^2(1 - 2\epsilon)F_{\mu\nu}^4(x) + \frac{5\epsilon - 4}{30}((\mathcal{D}_\mu^2 F_{\mu\nu}(x))^2 + (\mathcal{D}_\nu^2 F_{\mu\nu}(x))^2) + \frac{2\epsilon - 1}{3}\mathcal{D}_\mu^2 F_{\mu\nu}(x)\mathcal{D}_\nu^2 F_{\mu\nu}(x) + \frac{1 - 2\epsilon}{4} \times (\mathcal{D}_\mu \mathcal{D}_\nu F_{\mu\nu}(x))^2 \right) \right] + O(a^{10}, g^4), \quad (23)$$

into which we substitute the instanton solution to find that

$$S^{\text{inst}}(\epsilon) = \frac{8\pi^2}{g^2}\left[1 - \frac{\epsilon}{5}\left(\frac{a}{\rho_{\text{inst}}}\right)^2 + \frac{14\epsilon - 17}{210}\left(\frac{a}{\rho_{\text{inst}}}\right)^4 \right]. \quad (24)$$

As in Eq. (21), negative values of ϵ will result in a positive leading error term, and should preserve instantons.

We introduce the over-improvement parameter into the stout-link smearing algorithm by modifying the link combinations used in Eq. (9). Whereas the original $C_\mu(x) = \rho_{\text{sm}} \sum \{1 \times 1 \text{ paths touching } U_\mu(x)\}$, the modified stout-link $C_\mu(x)$ has the form

$$\mathcal{C}_\mu(x) = \rho_{\text{sm}} \sum \left\{ \frac{5 - 2\epsilon}{3}(1 \times 1 \text{ paths touching } U_\mu(x)) - \frac{1 - \epsilon}{12}(1 \times 2 + 2 \times 1 \text{ paths touching } U_\mu(x)) \right\}, \quad (25)$$

and the definition of the smearing parameter ρ_{sm} is unchanged. Note that both forward and backward horizontally orientated rectangles are included in the 2×1 paths, such that $\Omega_\mu(x)$ resembles the local action.

B. Tuning

Of course, this now begs the question: How negative should ϵ be in order to preserve instantons? Perez *et al.* reported a value of $\epsilon = -1$ to preserve instantons, and indeed it does. However, just as positive values of ϵ can shrink instantons, so too can negative values cause instantons to grow. Just as small instantons can fall through the lattice, big instantons can grow so large that they are destroyed by the smoothing procedure [19]. Additionally, one does not want to unnecessarily distort the instanton-like objects in the gauge field. Care must therefore be taken not to choose a value of ϵ that is too negative.

In order to quantify the selection of ϵ, we propose that one considers the ratio $S(\epsilon)/S_0$, where $S_0 = 8\pi^2/g^2$ is the single instanton action. Ideally $S(\epsilon)/S_0$ should be equal to 1 for all values of the instanton size, ρ_{inst}, as it is in the continuum.

Plots of $S(\epsilon)/S_0$ versus ρ_{inst} for the Wilson and Symanzik actions are shown in Fig. 1. Note that it is the slope of the curve that will govern whether an instanton shrinks or grows. Although the Symanzik action is closer to the ideal action than the standard Wilson action, the slope is still positive for all ρ_{inst} and using this action will shrink instantons.

The goal is now to select a value of ϵ that results in the flattest line possible, thereby ensuring the stability of instantons. A plot for three different values of ϵ is shown in Fig. 2. With $\epsilon = -1$ the curve for $\rho_{\text{inst}} > 1a$ is similar to the mirror image of the Wilson action. For $\rho_{\text{inst}}/a > 1.5$, $\epsilon = -0.25$ and -0.35 give curves closer to the ideal, however as $|\epsilon|$ is decreased the maximum occurs at larger ρ_{inst}. Since it is the slope that is responsible for how an

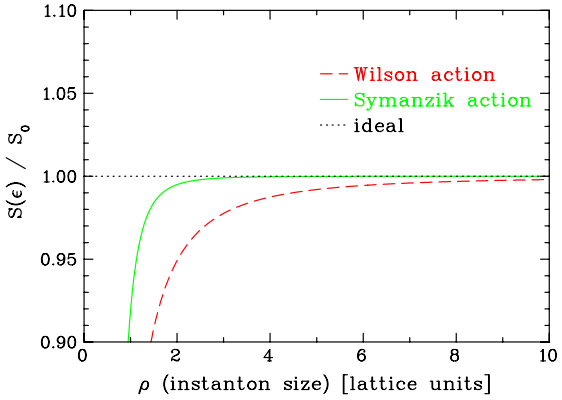

FIG. 1 (color online). $S(\epsilon)/S_0$ versus the instanton size for the Wilson and Symanzik improved actions. The ideal action would produce a flat line at $S(\epsilon)/S_0 = 1$. The positive slope on both curves means that instantons will shrink if the Wilson or Symanzik actions are used to smooth the gauge field.

instanton's size changes, the maximum of $S(\epsilon)$ gives the dislocation threshold of the smearing algorithm. Assuming that any topological excitation of length $\geq 2a$ is not an unphysical UV fluctuation or lattice artifact, one should aim for a dislocation threshold of $\sim 2a$.

Given this, we propose that a value of $\epsilon = -0.25$ will be sufficient. This choice gives a dislocation threshold of $\sim 2.0a$, and a curve that is mostly flat down to values of $\rho_{\text{inst}} \sim 1.7a$. The action $S(\epsilon)/S_0$ is also very close to the ideal.

In Fig. 3 we provide a comparison of the Perez *et al.* over-improved action, our over-improved action $S(-0.25)$, and the standard Wilson action. It is clear that $S(-0.25)$ will produce the best results, and presents an important advance beyond the work of Ref. [13].

Given a value for ϵ, one can find a suitable value for the smearing parameter, ρ_{sm}. Starting from an arbitrary value, systematically increase ρ_{sm} until u_0 (the mean-plaquette value) no longer increases when smearing. This value sets an upper threshold for ρ_{sm} and one should then choose

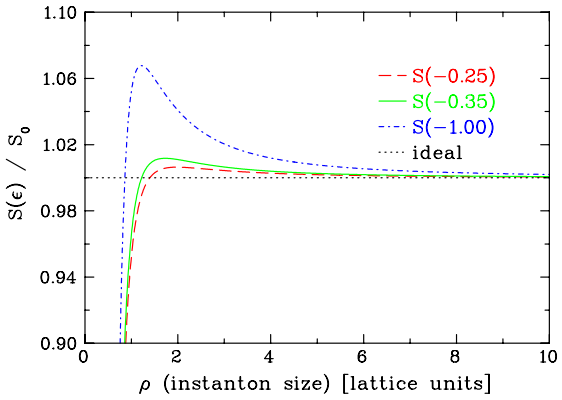

FIG. 2 (color online). $S(\epsilon)$ for three different values of ϵ. The larger $-\epsilon$ is made the further the curve moves from the ideal behavior and the sharper the maximum.

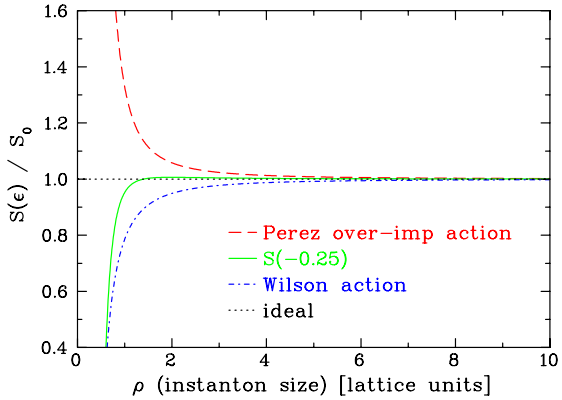

FIG. 3 (color online). A comparison of $S(\epsilon)/S_0$ for the Perez over-improved action, our over-improved action $S(-0.25)$, and the standard Wilson action.

some ρ_{sm} suitably below this threshold. In what follows we use a value of $\rho_{\text{sm}} = 0.06$. A typical value for standard stout-link smearing is $\rho_{\text{sm}} \approx 0.1$. The over-improved algorithm is more sensitive to the smearing parameter than standard smearing because of the larger loops used in the smoothing procedure.

V. ALGORITHM COMPARISONS

Given the selection of $\epsilon = -0.25$, it is now important to make a comparison of over-improved stout-link smearing with standard stout-link smearing. We are primarily concerned with the stability of the topological charge under smearing, and the structure of the gluon fields after smearing.

We use two sets of gauge fields for this study. First, an ensemble of large 28×96 dynamical MILC lattices [14,15], with light quark masses; $am_{u,d} = 0.0062$, $am_s = 0.031$. We will also use a quenched MILC ensemble of the same size and lattice spacing $a = 0.09$. The gauge fields were generated using a Tadpole and Symanzik improved gauge action with $1 \times 1 + 1 \times 2 + 1 \times 1 \times 1$ terms and an AsqTad staggered dynamical fermionic action for the $2 + 1$ flavors of dynamical quarks.

We also use quenched CSSM gauge fields created with the $\mathcal{O}(a^2)$ mean-field improved Lüscher-Weisz plaquette plus rectangle gauge action [20] using the plaquette measure for the mean link. The CSSM configurations are generated using the Cabibbo-Marinari pseudo-heat-bath algorithm [21] using a parallel algorithm with appropriate link partitioning [22]. To improve the ergodicity of the Markov chain process, the three diagonal SU(2) subgroups of SU(3) are looped over twice [6] and a parity transformation [23] is applied randomly to each gauge field configuration saved during the Markov chain process.

A. Topological charge

Let us first consider the evolution of the total topological charge of a gauge field under stout-link smearing. Typical

studies in the past have rated a smearing algorithm's success by its ability to generate and maintain an integer charge. We will also use this test to evaluate the effectiveness of the smearing procedures. It should be noted that we will be smoothing extremely large $28^3 \times 96$ lattices. Because of the vast amount of nontrivial topological charge field fluctuations present, it will take a lot of smoothing to generate a stable charge.

Figure 4 provides a sample of 4 different gauge fields smeared by standard ($\epsilon = 1$), Symanzik improved ($\epsilon = 0$), and over-improved ($\epsilon = -0.25$) stout-link smearing. The first two are $28^3 \times 96$ quenched MILC gauge fields, the third is a $28^3 \times 96$ light dynamical MILC field, and the last is a smaller $16^3 \times 32$ quenched field.

The top graph shows an example of the over-improved stout-link smearing producing a stable result. In this instance, the standard stout-link smearing curve is fluctuating widely, and is unable to reach a stable charge within 200 sweeps of smearing. The Symanzik improved smearing is better in that it stabilizes at around 120 sweeps; however the over-improved stout-link smearing is clearly superior, stabilizing 50 sweeps earlier. At around 70–120 sweeps there must exist a small instanton-like object that has been removed by the errors in the standard and improved smearing algorithms, but preserved by the tuned over-improved stout-link smearing.

The second graph is another typical example of what one sees when using the three different smearing algorithms. The standard stout-link smearing curve is still clearly the worst of the three, fluctuating the most. Meanwhile, the Symanzik and over-improved smearings are fairly similar in their behavior. Both stabilize at the same integer charge, but the over-improved algorithm stabilizes earlier. This is also the case in the third graph.

The final graph is a sample of a $16^3 \times 32$ lattice. It is shown here to represent how it is generally easier to smooth a smaller gauge field. For the larger lattices, their larger size means that there is a greater probability of finding an unstable topological object and it becomes more difficult to achieve integer charges rapidly.

These four graphs all demonstrate the benefits of using an improved smearing algorithm over the standard stout-link smearing commonly used in the field at present. Over-improved stout-link smearing typically provides a topological charge that is stable over hundreds of smearing sweeps, and one that approaches an integer much more rapidly than with conventional stout-link smearing.

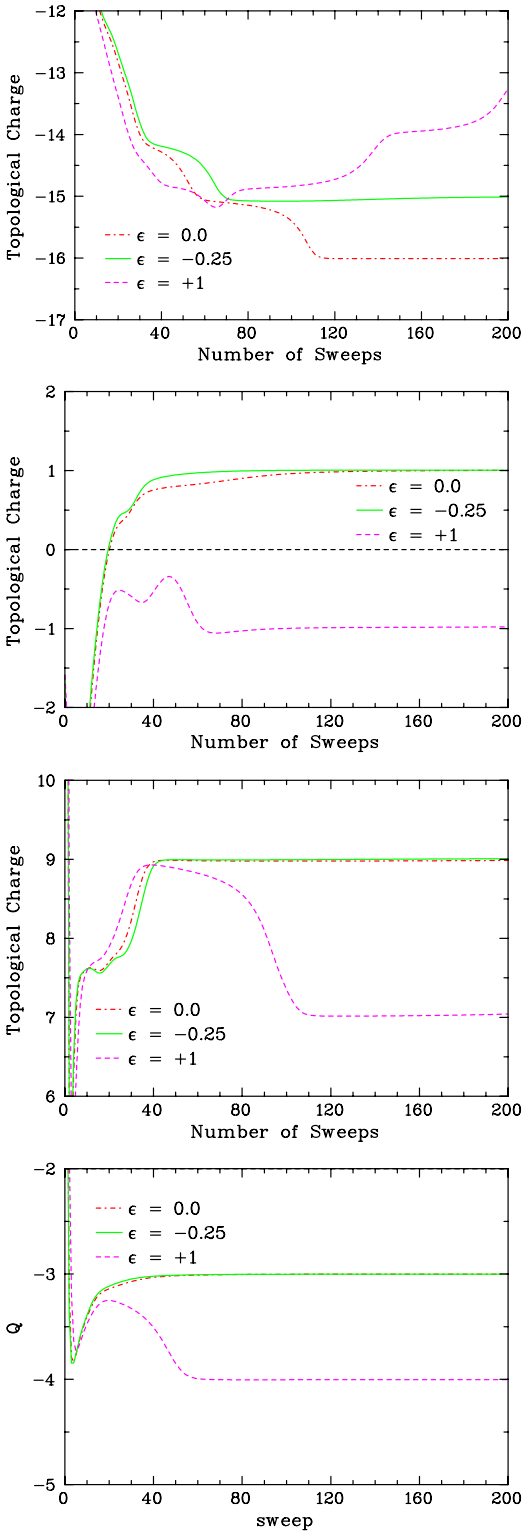

FIG. 4 (color online). Plots showing how the topological charge evolves under standard ($\epsilon = 1$), Symanzik improved ($\epsilon = 0$), and over-improved ($\epsilon = -0.25$) stout-link smearing. The two top graphs are from an ensemble of 28×96 quenched gauge fields. The third graph is from an ensemble of 28×96 dynamical fields with light quark masses. The bottom is a smaller 16×32 quenched gauge field. The features of the graphs are explained in the main text.

B. Topological charge density

For the next part of the analysis we will directly observe the topological charge density of the gauge fields. Our aim is to observe the differences in the gauge fields revealed by using the standard and over-improved stout-link smearing algorithms.

To achieve this we will require a gauge field where the final topological charges from the two smearing procedures differ. The topological charge, as a function of the number of smearing sweeps, is shown in Fig. 5. It appears as though an anti-instanton is being destroyed by the standard stout-link smearing from about 20 sweeps onwards. It will be interesting to visualize $q(x)$ in this region to see if we can observe this behavior. Indeed, by considering the differences in the charge density, we are able to locate the "anti-instanton" that is removed by the standard stout-link smearing.

In Fig. 6 we show how the anti-instanton is affected by the standard stout-link smearing, and in Fig. 7 we have the corresponding charge density from the over-improved stout-link smearing. The pictures present a single slice of the charge density of the 4D lattices as they evolve under the stout-link smearing.

After 30 sweeps we see that both smearing methods have revealed a similar vacuum structure. The effects of the errors in the standard smearing are first seen after 33 sweeps, when the anti-instanton-like object on the right begins to unwind in the upper-right corner. Here the charge density is approaching zero and therefore is not rendered. In a few sweeps the action density in this region will manifest itself in the opposite winding, largely eliminating the total topological charge. The net effect is to suggest that the instanton-like object on the right invades the neighboring negative object. However, the change in Q indicates that this is not an instanton-anti-instanton annihilation. At this point the majority of the negative topological charge density is lost and the total Q for the configuration approaches 1. This kind of phenomenon should not be seen as filtering is applied to a lattice, and indeed it does not occur when using the over-improved smearing.

After 36 sweeps the opposite winding has grown in size and it continues to grow in size as more smearing is applied to the lattice. After 39 sweeps the negatively charged object has all but disappeared. Although not shown, eventually the neighboring positive object expands to engulf the region originally occupied by the negatively charged excitation.

Here we have directly demonstrated how the discretization errors in the standard stout-link smearing algorithm have resulted in an erroneous picture of the vacuum, and

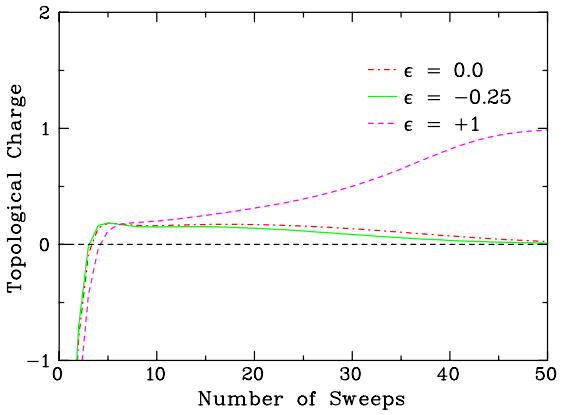

FIG. 5 (color online). The topological charge evolution under smearing for a 16×32 lattice. We see that when standard smearing ($\epsilon = 1$) is used an anti-instanton is destroyed at around 20–40 sweeps. Visualizations of the topological charge density in this region are discussed in the following text.

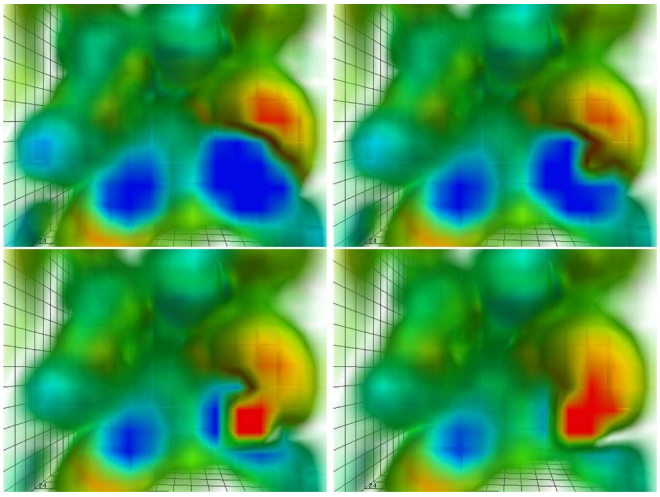

FIG. 6 (color online). The evolution of the topological charge density for various sweeps of standard stout-link smearing. The sweeps shown are: 30 (top), 33, 36, 39 (bottom). We see that a rather large anti-instanton is unstable under this smearing and is removed from the lattice, presenting an erroneous view of the vacuum. In color: blue to green represents negative topological charge, and red to yellow represents positive. In gray scale: dark regions represent negative topological charge, and the lighter regions represent positive.

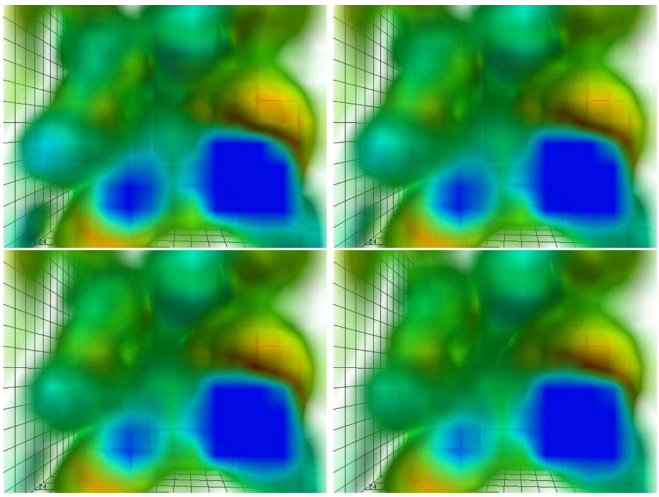

FIG. 7 (color online). A visualization of the topological charge density of the same gauge field shown in Fig. 6, this time with over-improved stout-link smearing. We see that in this case the anti-instanton in the lower right corner of the lattice is stable under smoothing, and remains stable for at least 200 sweeps.

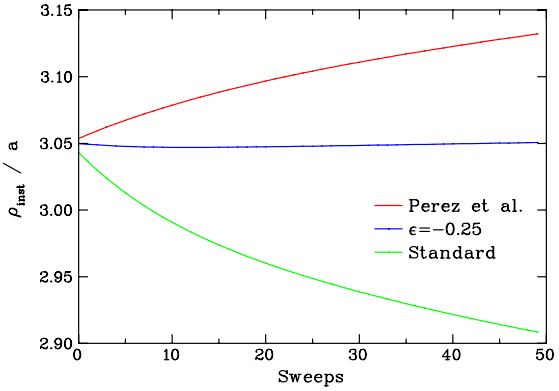

FIG. 8 (color online). The size evolution of single instanton under three different types of smearing. $\epsilon = 0.25$ refers to our over-improvement scheme, while Perez *et al.* denotes a stout-link implementation of their over-improvement method. Standard refers to standard unimproved stout-link smearing. The instanton is only stable under our proposed over-improvement scheme.

how by modifying these errors in the over-improved algorithm we are able to present a more accurate representation of the vacuum.

C. Single instanton evolution

We can also contrast the effects of different smearing algorithms by smearing a single instanton gauge field configuration. We create an instanton in singular gauge [24] and avoid Nahm-transform issues [19] via the action appearing at the boundaries of the lattice. Given that over-improved stout-link smearing with $\epsilon = -0.25$ has a dislocation threshold of about $2a$, we generate a gauge field containing a single instanton of size $\rho_{\text{inst}} = 3a$.

We compare our over-improved smearing against standard stout-link smearing and a stout-link implementation of the Perez *et al.* over-improvement scheme. An instanton of this size should stay relatively constant under over-improved smearing at $\epsilon = -0.25$. From Fig. 3 we anticipate that the Perez *et al.* over-improvement scheme will cause the instanton to grow in size. Similarly, standard stout-link smearing is expected to shrink the instanton. The size of the instanton is monitored by fitting the classical instanton action profile to the lattice action density in a 3^4 hypercube located at the center of the instanton.

The instanton's size evolution is presented in Fig. 8. We see that the instanton's size has remained constant under over-improved smearing. As predicted, Perez *et al.*'s implementation of over-improvement has caused the instanton to grow. In a study of QCD vacuum structure this would lead to an over-estimation of instanton sizes in the vacuum. Also as predicted, using standard stout-link smearing has caused the instanton to shrink. Further smearing would destroy the instanton. This calculation showcases the obvious need for over-improvement in the stout-link smearing algorithm.

VI. CONCLUSION

We have demonstrated how to define an over-improved stout-link smearing algorithm, with the aim of preserving instanton-like objects on the lattice. To the best of our knowledge, this is the first time link paths beyond the staple have been included in the stout-link smearing algorithm.

Using maximally local improvement we presented a new quantitative method of selecting a suitable value of the parameter ϵ. With the procedure defined, we demonstrated the success of the over-improved stout-link algorithm in preserving topological structures which were destroyed when using the standard stout-link smearing algorithm. This was done by analyzing both the topological charge and through visualizations of the topological charge density. We also performed a comparison of the over-improved smearing method with standard methods by smoothing a single instanton of size $\rho_{\text{inst}} = 3.0$. Over-improved stout-link smearing is the only algorithm capable of smoothing an instanton of this size without distorting it.

This paper highlights the need for improvement schemes to be incorporated into today's modern smearing algorithms. Over-improved stout-link smearing can be used in future studies of vacuum structure or other similar applications, where preserving topology on the lattice is important. Of particular interest is a quantitative comparison with the overlap-Dirac measure of topological charge density [25], and the impact of dynamical fermions on QCD vacuum structure [26].

ACKNOWLEDGMENTS

We thank Waseem Kamleh for his assistance in interfacing with his MPI Colour Orientated Linear Algebra (COLA) library. We also thank the Australian Partnership for Advanced Computing (APAC) and the South Australian Partnership for Advanced Computing (SAPAC) for generous grants of supercomputer time which have enabled this project. This work is supported by the Australian Research Council.

[1] B. Berg, Phys. Lett. **104B**, 475 (1981).
[2] M. Teper, Phys. Lett. **162B**, 357 (1985).
[3] E.-M. Ilgenfritz, M. L. Laursen, G. Schierholz, M. Muller-Preussker, and H. Schiller, Nucl. Phys. **B268**, 693 (1986).

[4] M. Falcioni, M. L. Paciello, G. Parisi, and B. Taglienti, Nucl. Phys. **B251**, 624 (1985).
[5] M. Albanese *et al.*, Phys. Lett. B **192**, 163 (1987).
[6] F. D. R. Bonnet, D. B. Leinweber, A. G. Williams, and J. M. Zanotti, Phys. Rev. D **65**, 114510 (2002).
[7] A. Hasenfratz and F. Knechtli, Phys. Rev. D **64**, 034504 (2001).
[8] C. Morningstar and M. J. Peardon, Phys. Rev. D **69**, 054501 (2004).
[9] S. Durr, arXiv:0709.4110.
[10] K. Symanzik, Nucl. Phys. **B226**, 187 (1983).
[11] P. de Forcrand, M. Garcia Perez, and I.-O. Stamatescu, Nucl. Phys. B, Proc. Suppl. **47**, 777 (1996).
[12] S. O. Bilson-Thompson, D. B. Leinweber, and A. G. Williams, Ann. Phys. (N.Y.) **304**, 1 (2003).
[13] M. Garcia Perez, A. Gonzalez-Arroyo, J. Snippe, and P. van Baal, Nucl. Phys. **B413**, 535 (1994).
[14] C. W. Bernard *et al.*, Phys. Rev. D **64**, 054506 (2001).
[15] C. Aubin *et al.*, Phys. Rev. D **70**, 094505 (2004).
[16] K. G. Wilson, Phys. Rev. D **10**, 2445 (1974).
[17] C. W. Bernard and T. A. DeGrand, Nucl. Phys. Proc. Suppl. **83**, 845 (2000).
[18] A. A. Belavin, A. M. Polyakov, A. S. Shvarts, and Y. S. Tyupkin, Phys. Lett. **59B**, 85 (1975).
[19] S. O. Bilson-Thompson, D. B. Leinweber, A. G. Williams, and G. V. Dunne, Ann. Phys. (N.Y.) **311**, 267 (2004).
[20] M. Luscher and P. Weisz, Commun. Math. Phys. **97**, 59 (1985).
[21] N. Cabibbo and E. Marinari, Phys. Lett. **119B**, 387 (1982).
[22] F. D. R. Bonnet, D. B. Leinweber, and A. G. Williams, J. Comput. Phys. **170**, 1 (2001).
[23] D. B. Leinweber, A. G. Williams, J.-b. Zhang, and F. X. Lee, Phys. Lett. B **585**, 187 (2004).
[24] D. J. Kusterer, J. Hedditch, W. Kamleh, D. B. Leinweber, and A. G. Williams, Nucl. Phys. **B628**, 253 (2002).
[25] E. M. Ilgenfritz *et al.*, Phys. Rev. D **77**, 074502 (2008).
[26] P. J. Moran and D. B. Leinweber, arXiv:0801.2016.